To be published in Optics Express:

Title:	Optimisation and scaling effect of dual-waveguide optical trapping in the SOI platform
Authors:	Xiangming Xu,David Thomson,Jize Yan
Accepted:	28 September 20
Posted	28 September 20
DOI:	https://doi.org/10.1364/OE.403151

Optimisation and scaling effect of dual-waveguide optical trapping in the SOI platform

XIANGMING XU,[1] DAVID J. THOMSON,[2] AND JIZE YAN[1,*]

[1]School of Electronics and Computer Science, University of Southampton, Southampton, SO17 1BJ, United Kingdom
[2]Optoelectronics Research Center, Zepler Institute for Photonics and Nanoelectronics, University of Southampton, Southampton, SO17 1BJ, United Kingdom
*J.Yan@soton.ac.uk

Abstract: Optical trapping has potential applications in biological manipulation, particle trapping, Raman spectroscopy, and quantum optomechanics. Among the various optical trapping schemes, on-chip dual-waveguide traps combine benefits of stable trapping and mass production. However, no systematic research has been conducted to optimise on-chip dual-waveguide traps so that the trapping capability is maximised. Here, a numerical simulation of an on-chip silicon on insulator (SOI) dual-waveguide optical trap based on Lumerical FDTD Solutions is carried out to optimise the on-chip dual-waveguide trap. It was found that the waveguide thickness is a crucial parameter when designing a dual-waveguide trap, and its optical trapping capability largely depends on the distance between the two waveguides. We show that the optimal waveguide thickness to achieve the maximum trapping capability generally increases with the gap distance, accompanied by a periodic feature due to the interference and the resonant effects within the gap. This optimal waveguide thickness and gap distance are analysed to have clear scaling effects over the input optical wavelength, which paves the way for the design and optimisation of dual-waveguide traps for various applications.

1. Introduction

The first demonstration of optical trapping was reported by Arthur Ashkin in 1970 [1] when he showed the first dual-beam optical trapping where two opposing equal-power laser beams were used, and particles were trapped stably at the equilibrium point. In 1986 [2], Ashkin reported the first single-beam gradient force optical trap, where a single focused laser beam was utilised to trap a particle in a liquid. Soon after that, the rapid development of optical traps led to the application of optical tweezers for trapping and manipulating viruses, cells, and bacteria, and it became a standard tool in biophysics [3]. Besides, optical traps are essential building blocks for levitated optomechanics [4,5], where dielectric particles are trapped by optical force and decoupled from the environment. The resulting ultra-high Q factor of the levitated particle makes it the most promising platform for application in high-sensitivity sensing [6–8] and test of quantum physics [9,10]. Among the two optical trapping schemes, single-beam optical trapping shows a limitation in the application for trapping large particles where the dominating radiation scattering force will overpower the gradient force and thus push the particle out of the trap. On the contrary, in dual-beam optical trapping, the optical gradient force is used to trap particles, while the axial radiation scattering forces from the two counter-propagating laser beams are balanced and thus make the optical trapping more stable. In the meantime, the particle trapping position can also be controlled by changing the relative power, frequency, or phase of the laser beams.

Various dual-beam optical traps have been demonstrated, either using optical fibres [11,12] or liquid waveguides [13], while yet unfit for mass production of trapping devices. Dual-waveguide trapping, which combines state of art micro-nano fabrication

technology and the dual-beam optical trapping scheme, enables such mass production and at the same time avoids any delicate mounting and alignment of optical fibres as in the conventional dual-beam trapping.

Long before the dual-waveguide trapping, the evanescent field of an optical waveguide has been used to attract particles to the surface of a waveguide using optical gradient force and propel the particles along the waveguide with radiation pressure force [14–16]. However, this kind of optical trapping generated from the exponentially decaying evanescent field cannot stably trap the particle at a fixed position. This is where dual-waveguide optical trapping can play a role. A variety of dual-waveguide optical trapping schemes have been proposed and experimentally demonstrated. In 2011, Jacob Caro and co-workers first proposed and numerically verified the dual-waveguide optical trapping scheme with two multimode strip Si_3N_4 waveguides launching counter-propagating beams into a fluidic channel [17]. Later on, they experimentally demonstrated dual-waveguide optical traps based on a composite SiO_2-Si_3N_4 waveguide structure called the TripleX platform [18–20], on which they successfully trapped polystyrene beads and realised on-chip single-beam Raman spectroscopy. Recently, They also proposed and demonstrated a multi-waveguides device for trapping and Raman spectroscopy [21]. Olav Gaute Hellesø demonstrated similar dual-waveguide optical traps using waveguide loops made of 150-180nm tantalum pentoxide (Ta_2O_5) on oxidised silicon substrates, where polystyrene microspheres and red blood cells were propelled along the waveguides and stably trapped in the gap area [22,23]. In the following years, they carried out on-chip optical trapping for Raman spectroscopy [24], lifting of particles [25], and they also used rib waveguides for on-chip optical trapping [26].

In the reports mentioned above, intensive numerical simulations have also been performed to study the field intensity profile, optical trapping force, and trapping potential acting on particles with different radii and under different gap distances. It was found that both the particle size and gap distance have significant effects on the trapping force and potential. The waveguide cross-section is manifestly another crucial geometric parameter, as it determines how the mode profile is distributed and how the guided waveguide mode is converted into the radiation mode outside the waveguide facet boundaries. However, no research has been conducted to systematically investigate the effect of waveguide geometry on trapping capability until now, particularly the waveguide thickness under the single-mode condition.

In this context, we here carry out numerical simulations of SOI dual-waveguide optical traps based on Lumerical FDTD solutions [27] to study the effect of single-mode waveguide thickness on the capability for trapping particles. We first present the capability for optical trapping using a dual-waveguide structure made from the SOI substrate. It is then found from simulations that the waveguide thickness is a crucial parameter when designing the trapping scheme, and the optimal waveguide thickness depends on the gap distance between waveguides. This dependence is characterised by a monotonically increasing trend composited with periodic features due to the interference effect. We also study the effect of wavelength and find that the optimal thickness shows a scaling effect over wavelength. Our simulation results provide comprehensive guidance for the design and optimisation of dual-waveguide optical traps in terms of wavelength, gap distance, and waveguide thickness.

2. Dual-waveguide optical trapping and simulation approach

2.1 Dual-waveguide configuration

The dual-waveguide optical trapping model used for the simulation in Lumerical's FDTD solutions is shown below in Fig. 1(a). Two identical rib waveguides made from an SOI substrate are separated by an intentionally designed gap with distance L. Compared to the TripleX and Ti_2O_5 platforms which have been used in previous dual-waveguide traps [18,26], the SOI substrate shows more advantages because it is commercially available at low cost and is complementary metal-oxide-semiconductor (CMOS) compatible. In addition, the state-of-

the-art silicon photonics technologies facilitate the integration of electronics, optics, and mechanics on the same wafer, in the same fabrication facility.

In the simulation, two in-phase mode sources, with the same power of 50mW each, are placed at 0.5μm from the end facet of the waveguides with opposite injection directions. The fundamental transverse electric (TE) mode shown in Fig. 1(b) is excited in each source. We set the material of the guided layer and bottom cladding layer to Silicon and SiO_2, respectively. Before running the simulation, the refractive index is fitted according to the material library of the Lumerical software. The background index of the model is set to be 1, which corresponds to the air or vacuum environment. A rib geometry is chosen because it can maintain the single-mode condition even in thick waveguides. The etching ratio, defined as the ratio of the etched thickness to the overall thickness of the silicon layer, is kept as a constant of 0.5, and the waveguide width is set to be $w = 0.87t$, which is the maximum value to maintain the single-mode condition [28]. The waveguide slab width is set to be 10 μm considering the higher order mode leakage into the slab, and the thickness of SiO_2 is set to be 2 μm.

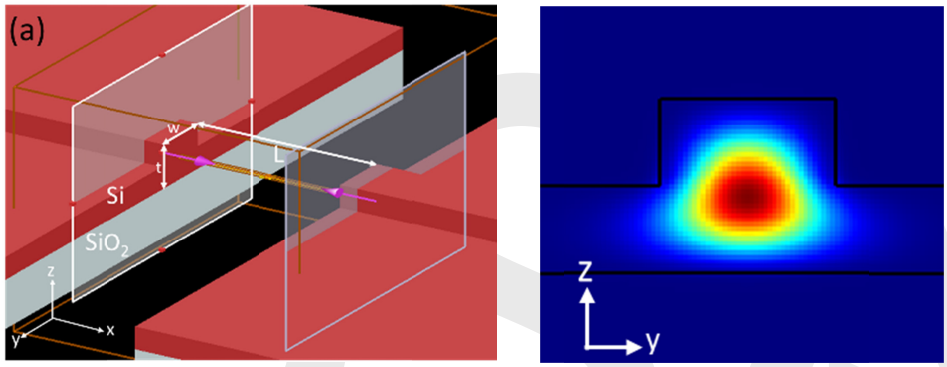

Fig. 1. (a) Schematic of the simulation model for the dual-waveguide optical trap. Two identical rib waveguides are separated by a gap distance L, and two in-phase mode sources with the same powers of 50mW are placed at 0.5μm from the end facet of the waveguides with opposite injection directions. To maintain single-mode condition the waveguide width is set to be $w = 0.87t$, where t is the thickness of the waveguide. (b)TE source mode profile of the rib waveguide.

We set the coordinate origin point to be at the centre of the gap in the x-direction, at the centre of the waveguide width in the y-direction and on the slab surface in the z-direction. The FDTD simulation domain is set to be 10 μm in both *y*- and *z*-direction. In the *x*-direction, the simulation domain is L + 3 μm. Perfectly matched layer (PML) is used as the boundary condition. A power monitor is placed at the x-axis within the gap to measure the optical intensity distribution between the waveguides. When implementing the FDTD simulation, a 50nm mesh size is used, which is proven to be fine enough to resolve the fields through the FDTD mesh convergence test.

2.2 Intensity field profile

The dual-waveguide trap with waveguides thickness t =2 μm and input wavelength λ =1550nm is first simulated to study the characteristics between the two waveguides. The simulated optical field profiles in the XY plane (Z=0) and XZ plane (Y=0), are shown in Fig. 2(a and b) for a gap distance L=1 μm, and in Fig. 2(c and d) for a gap distance L=3 μm. In the intensity field profiles, colours represent the intensity of the field. It can be found that both in the XY plane and XZ plane the light guided inside the waveguides diverges rapidly at the facet, and then interferes to generate several periodically distributed local maximum intensity points inside the gap area. There is one point for the gap distance L=1 μm and three points for

the gap distance L=3 μm. These hot points are the positions where particles can be trapped by the optical gradient force. The interference fringe can also be found in the waveguide, which is caused by the interference of propagating light and reflected light from the waveguide facet. Within the gap, the period deduced from the modulation patterns is in close agreement with the theoretical value of λ/2=775nm. When comparing the field profiles in XY plane and XZ plane, it is apparent that the beam leaving the waveguides in XZ plane is more divergent than in XY plane, since the confinement of the waveguide mode is tighter in the vertical direction than in horizontal direction.

The periodic pattern within the gap is generated by interferometric modulations from two aspects. Firstly, it is the interference between the propagating light transmitted out of one waveguide facet and the reflected light from the facet of another waveguide. Secondly, it is the interference between the two counter-propagation beams which come from the two mode sources and transmitted out of the end facets of the waveguides. Due to the much larger transmission over reflection at the air/silicon interface [29], the second type of interference dominates. Given the condition that the two mode sources are set in phase, there is a constructive interference effect at the centre due to the matched distances to the mode sources, thus the intensity at the centre is always a local maximum while changing the gap. This constructive interference also happens at locations in the x-axis where $x=\pm\frac{k\lambda}{2}, k = 0,1,2$ ....., in which the gap distance must be greater than $\frac{(2k+1)\lambda}{2}$. These points are further called the trapping points.

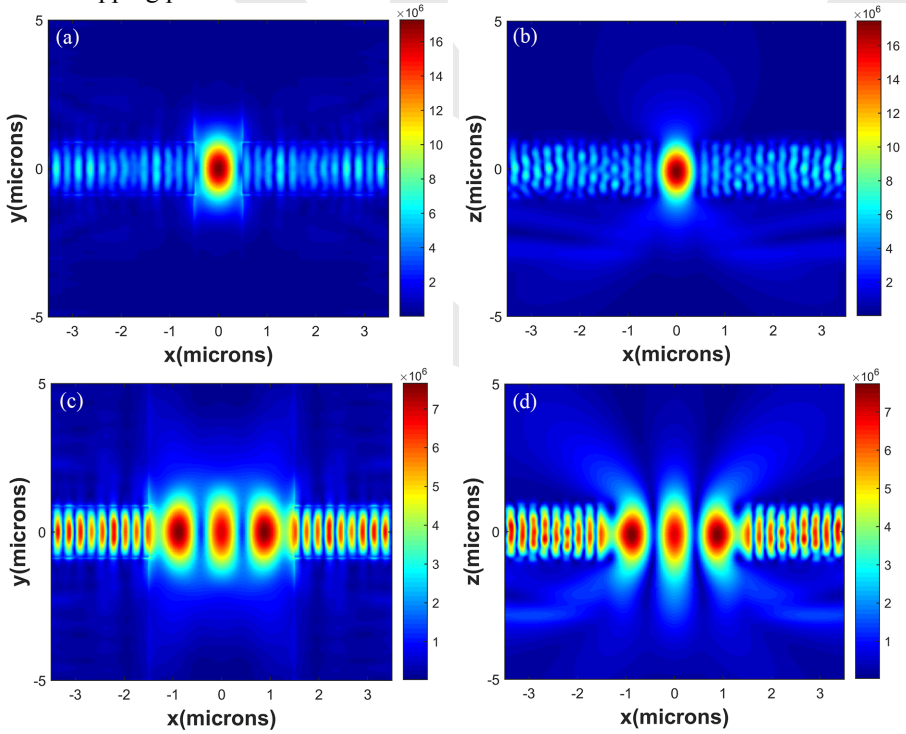

Fig. 2. (a and b) Field intensity profile for a gap distance L=1μm in XY plane and XZ plane, respectively. (c and d) Field intensity profile for a gap distance L=3μm in XY plane and XZ plane, respectively.

2.3 Optical trapping force, trapping potential and optical intensity

Assuming a dielectric particle is placed within the gap, the particle will be trapped to one of the trapping points owning to the optical gradient force pointing to the region with the highest optical intensity. Due to the conservative nature of the optical gradient force, a unique value

called trapping potential can be assigned to each location. The depth of the trapping potential well plays a crucial role in keeping the trapped particles within the optical trap and can be used to characterise the optical trapping capability. The deeper the potential well is, the more stable the optical trap becomes. According to Ashkin's stability criterion [2], the depth of the potential well has to be higher than $10k_bT$, where k_b is the Boltzmann constan and T is the temperature, to make the optical trapping capability strong enough to offset the effect of Brownian thermal vibration of the particle so that the particle can be stably trapped.

In Lumerical's FDTD Solutions, the optical force acting on a particle can either be calculated by integrating the Maxwell stress tensors (MST) over a cube around the particle or by calculating the volume integral of the time-averaged Lorentz force density for a cube enclosing the particle [30]. After that, the trapping potential can be calculated by integrating the optical force over the space of the particle. We here demonstrate an SOI dual-waveguide optical trap with waveguide thickness t=3.5μm and gap distance L=4μm, in which a silica sphere with 200nm diameter is trapped at the centre. The input optical wavelength is 1550nm and the applied power is set to be 50mW. The simulated optical force and trapping potential for the y-axis (Fig. 3(a)), z-axis (Fig. 3(b)) and x-axis (Fig. 3(c)) are plotted below respectively. In the figures, the resulting trapping potentials are normalized to K_bT ($T = 300K$).

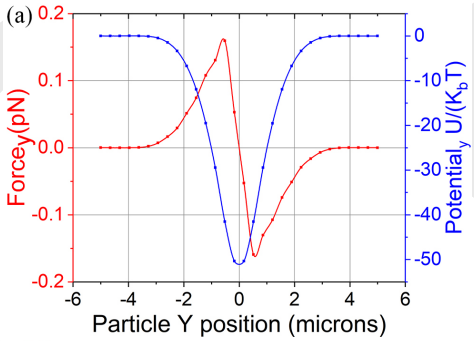

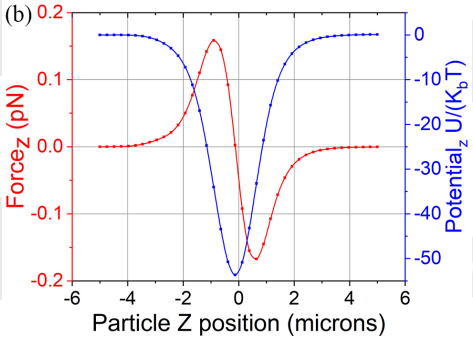

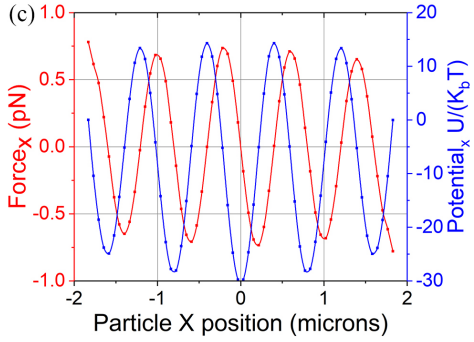

Fig. 3. (a, b and c) The simulated optical force and trapping potential for a silica sphere with 200nm diameter trapped at the centre of a dual-waveguide optical trap with waveguide thickness t =3.5μm and gap distance L =4μm in the y-axis, z-axis and x-axis respectively. Note that the applied optical power is 50mW each.

It can be found from Fig. 3(a and b) that a stable optical trap for 200nm particle can be formed along the y-direction and z-direction with a 50mW applied power. The optical force is linear around the centre and the shows a restoring character attracting the particle to the centre. While in the X direction, multiple trapping points are generated along the x-axis, which agrees with the field intensity pattern analysis in Sec. 2.2. According to the criteria of stable trapping, the potentials in all the three directions are deep enough to overcome the particle Brownian motion and thus form a stable optical trap.

However, the process of calculating optical force and trapping potential shown above can only be implemented by parametrically sweeping the location of the particle to get the optical force acting on the particle at each position, which will require significant computational resources. The simulation time may even increase by orders of magnitude if we also want to study the effect of gap distance and waveguide thickness. Therefore, another figure of merit to quickly assess the optical trapping capability is desired.

The particles interacting with light can be treated as point dipole charges in an electric field when the particle size falls into the Rayleigh scattering regime, in which the size of the particle is much smaller than the optical wavelength. The time-averaged Lorentz force acting on this dipole charge can be written as [31],

$$F(\boldsymbol{r}) = \pi {n_2}^2 \varepsilon_0 a^3 \left(\frac{m^2 - 1}{m^2 + 2} \right) \nabla \left| E(\boldsymbol{r}) \right|^2, \tag{1}$$

Where n_2 is the refractive index of the surrounding medium, ε_0 is the dielectric constant in a vacuum, a is the radius of the particle, m is the relative refractive index between the particle and the surrounding medium, E is the electric field amplitude in an empty trap, $\boldsymbol{r} = (x, y, z)$ is the location of the centre of the particle. Substituting the relation of the optical intensity and the electric amplitude shown below,

$$I(\boldsymbol{r}) = \frac{n_2 \varepsilon_0 c}{2} \left| E(\boldsymbol{r}) \right|^2, \tag{2}$$

We find,

$$F(\boldsymbol{r}) = \frac{2\pi n_2 a^3}{c} \left(\frac{m^2 - 1}{m^2 + 2} \right) \nabla I(\boldsymbol{r}), \tag{3}$$

In which c is the speed of light in vacuum and I is the optical intensity. It is found that the optical force is proportional to the gradient of the optical field intensity and points towards the region of the highest field intensity, which produces a restorative force and attracts the particles. The optical trapping potential can then be derived at any point by integrating the time-averaged optical force according to,

$$U(\mathbf{r_0}) = -\int_{\infty}^{\mathbf{r_0}} \boldsymbol{F}(\boldsymbol{r}) \cdot d\boldsymbol{r} = -\frac{2\pi n_2 a^3}{c} \left(\frac{m^2 - 1}{m^2 + 2} \right) I(\mathbf{r_0}), \tag{4}$$

In which we assume $U(\infty) = 0$. From Eq. (4), the optical trapping potential is linearly proportional to the field intensity I, which means the optical trapping capability can be characterised by the optical intensity in the trapping point if the Rayleigh scattering condition is matched.

In this paper, we only study the particles with dimensions from tens of nanometer to several hundred nanometers that match the Rayleigh particle condition for our simulation wavelength. Therefore, a dual-waveguide optical trap configuration without a particle is used to simulate the trapping characteristics of the dual-waveguide optical trap. In the meantime,

the optical intensity I is also linearly proportional to the square of the electric field amplitude$|E|^2$ from Eq. (2). Thus, $|E|^2$ is chosen to represent the optical intensity within the gap and to work as the figure of merit to assess the trapping capability under different waveguide thicknesses. It has to be understood that this depends on the prerequisite that the particle size falls into the Rayleigh scattering regime. For larger particles out of this regime, the optical potential is complicated and are not just related to the optical field intensity, which is beyond the scope of this paper.

3. Intensity field profile over different waveguide thickness

We start by analysing the optical field distribution features within the gap of the optical traps under different waveguide thicknesses. When the wavelength λ =1550nm, the simulated optical field intensity profiles in the x-axis for dual-waveguide traps with waveguide thicknesses from 0.5μm to 4μm are shown below in Fig. 4(a), (b), (c), (d) for gap distance L=0.775μm, L=2.325μm, L=3.875μm, L=5.425μm, respectively. Those four gap distance theoretically meet the standing wave condition when the wavelength is λ =1550nm. It can be found the number of trapping points, namely the local intensity maximum points, increases with the gap distance L. In each of the trapping points along the x-axis, it is apparent that there is a waveguide thickness value in which the optical intensity reaches its local highest, meaning that we can find an optimal waveguide thickness which maximises the optical intensity and trapping capability.

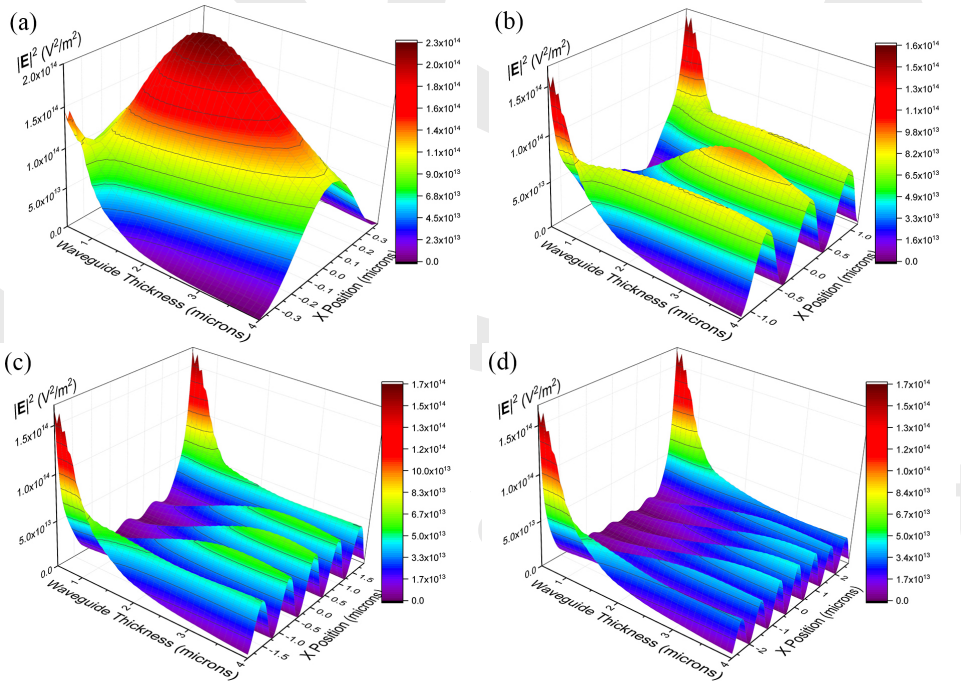

Fig. 4. Field intensity profile in the x-axis for dual-waveguide trap with waveguide thickness from 0.5μm to 4μm when (a) the gap distance L=0.775μm. (b) the gap distance L=2.325μm. (c) the gap distance L=3.875μm. (d) the gap distance L=5.425μm. The grey line in the figures show the contour map of the optical intensity $|E|^2$

When looking at the field intensity near the edges of the gap in the four figures, it is interesting to note that the intensity curves at the edges almost align with each other for different gap distances and in the meantime decreases with the waveguide thickness for each curve. This is because the input power of the two mode sources is set to be the same for different waveguide thickness, and thus the field intensity is reversely proportional to the

waveguide cross-section area, which means waveguide with smaller thickness has higher field intensity. Besides, across the air/silicon interface, i.e. the end of the waveguide, the field intensity distribution is continuous, and this makes the intensity at the two edges of the gap dependant only on the waveguide thickness and independent of the gap distances between two waveguides. Therefore, the values of the intensity at the edge of the gap are equal for configurations with the same waveguide thickness. On the other hand, the radiation loss within the gap increase with gap distance, so the overall intensity inside the gap decreases with the gap distance. This makes the peaks near the edge of large distance gap more prominent than the counterpart in small distance gap. Therefore, two high peaks on the two edges of the gap are observed clearly in the case of small waveguide thickness in Fig. 4(b, c and d). As a comparison, the peaks in Fig. 4(a) is not that prominent due to the high-intensity hot spot inside the gap.

What deserves noting is the second-highest intensity area in Fig. 4(a) and the highest intensity areas in Fig. 4(b, c, and d). They are at the edge of the gap area when the waveguide thickness is small. There are two theoretical trapping points close to the edge of the gap at x $\approx \pm 0.775\mu$m for Fig. 4(b), x$\approx \pm 1.55$ μm for Fig. 4(c), x$\approx \pm 2.325\mu$m for Fig. 4(d), at the configuration with larger waveguide thickness, where the local maximum intensity points exist. Particles can be thus trapped here rather than attracted to the end facet. As for the case of small waveguide thickness, however, the intensity at the edge of the gap is too high that the theoretical trapping points disappear, and particles would be attracted to the end facet of the waveguides. This feature is very meaningful in overcoming the drawbacks in traditional dual-waveguide optical trapping, where particles can be easily attracted to the end of the waveguide, by properly designing the waveguide thickness and gap distance.

4. Optimal waveguide thickness for optical trapping

When the wavelength is λ =1550nm, we here conducted a parametric sweep of the gap distance L and waveguide thickness t in FDTD Solutions, to study the effect of these two parameters on the field intensity at the trapping points, which represents the trapping capability there. The waveguide thickness t is swept from 0.5μm to 4μm, and the gap distance L is swept from 0.5μm to 6.2μm. During the simulation, we elaborately set the value of each input mode source electric amplitude for optical traps with different waveguides thicknesses, to ensure that each input power of the two in-phase sources is always the same at 50mW. The input power is calculated by the built-in function "sourcepower" of FDTD Solutions. By doing this we can eliminate the effect of the input optical power on the trapping capability, and focus on the study of the impact of waveguide thickness and gap distance.

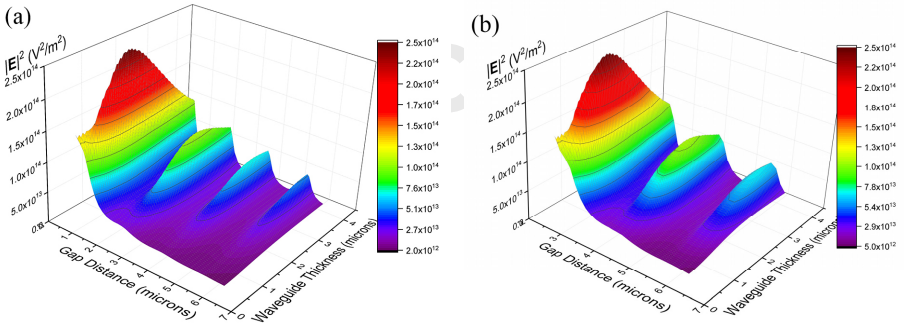

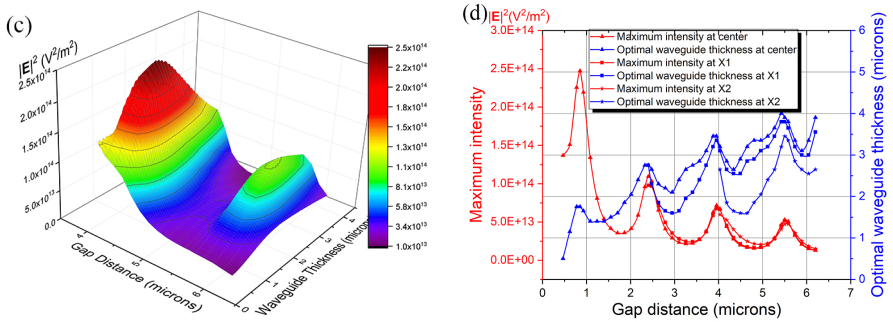

Fig. 5. When the wavelength is λ =1550nm (a,b, and c) The field intensity as a function of the gap distance L and the waveguide thickness t at the centre, X1, X2, respectively. The colour represents the optical intensity. (d) The extracted maximum optical intensity and optimal waveguide thickness t_{op} as a function of the gap distance L at the centre, X1, X2. The blue curves represent the extracted data for the optical waveguide thickness t_{op}, while the red curves indicate the corresponding maximum optical intensity. The curves with triangular, rectangular, and star shape symbols represent the data for the trapping point at the centre, X1, and X2, respectively.

As analysed above, there are multiple trapping points within the gap. For the trapping points located at x=0, x=$\pm\frac{\lambda}{2}$, x=$\pm\lambda$, further called the centre, X1 and X2, Fig. 5(a), (b), (c) shows the relation of the field intensity as a function of the gap distance L and the waveguide thickness t respectively. We found from the 'ridge' like intensity surfaces that the field intensity generally decreases with the gap distance L in all three of the graphs. This is intuitive because a larger gap distance means more radiation mode energy is diverged and lost to the outside medium environment, leading to a lower optical intensity within the gap. At the position of the ridges, however, periodically local maximum intensity points along the gap distance direction can be found, which are attributed to the constructive interference of light between the two waveguide facets when the gap distance L matches the standing wave condition. It is also apparent that, for each gap distance L, there is a value of waveguide thickness t that can maximise the optical intensity, which is called the optimal waveguide thickness t_{op}. These figures also show that t_{op} is not a constant but rather dependent on the gap distance L. This can be understood by considering the dual-waveguide optical trap as a coupled-resonator model which has been introduced in [29]. In the coupled-resonator model, the maximum intensity within the resonator occurs when the critical coupling condition is matched, namely $\kappa_e = \kappa_i$, where κ_e refers to the loss rate associated with the input coupling, and κ_i refers to the remaining internal loss. In the dual-waveguide configuration described here, κ_e and κ_i are determined by waveguide thickness t and gap distance L. Even though the accurate numerical relationship between them is still unclear and currently under exploration, what is certain is that there is an optimal combination of waveguide thickness t and gap distance L according to the coupled-resonator theory, thus we can find an optimal waveguide thickness t_{op} for each gap distance L to maximise the intensity.

Extracted from the field intensity profiles in Fig. 5(a, b and c), Fig. 5(d) shows the maximum optical intensity and the corresponding optimal waveguide thickness t_{op} over the gap distance L at the trapping points at the centre, X1, X2. From the red curves representing the maximum optical intensity, periodic peaks along with a descending trend are observed. The periodic peaks come from intensity enhancement due to standing wave modulation, while the descending trend is caused by the increased optical energy loss to the environment with gap distance. It can also be found that the maximum intensity curves at the center, X1, and X2 align with each other very well, meaning the maximum trapping capability for the center, X1 and X2 are almost at the same level.

From the blue curves representing the optimal waveguide thickness t_{op}, we found that t_{op} generally increases with the gap distance, which indicates a thicker waveguide is preferred to maximise the trapping capability with a larger gap distance. However, the trends do not monotonically increase but rather change with a periodic feature whose period matches perfectly with the red curves for maximum intensity.

Looking into the difference between the optical waveguide thickness curves for the three trapping points, it is found that the t_{op} for the trapping point at the centre is larger than that for the trapping points at X1 and X2. Nevertheless, when the gap distance matches the standing wave condition, the t_{op} is generally consistent with each other.

5. Scaling effect over the wavelength

In the above analyses, we set the wavelength λ to be 1550nm. However, other wavelengths can also be used in optical trapping applications, such as 785nm which has been used for Raman spectroscopy excitation in optical trapping demonstrated in [18]. In addition, the input optical wavelength can be easily tailored to maximise the trapping capability through a tunable laser, for which we must first find out what role the input wavelength plays in the design of dual-waveguide optical traps. Therefore, in addition to the sweep of the waveguide thickness t and the gap distance L in Section 4, we here add another parametric sweep of the wavelength λ from 1100nm to 2000nm, to study the effect of wavelength on the optimal waveguide thickness t_{op}. Again, waveguide thickness t is swept from 0.5μm to 4μm, and gap distance L is swept from 0.5μm to 6.2μm. The input optical power is set to be the same at 50mW for each mode source to eliminate the effect of the input power.

To take into account the effect of optical wavelength, we normalise the geometric value, namely the gap distance L and the waveguide thickness t, to the input wavelength λ. Fig. 6(a, b, and c) show the normalised optimal waveguide thickness $t_{op\_nor} = t_{op}/\lambda$ as a function of the normalised gap distance $L_{nor} = L/\lambda$ at the trapping point at the centre, X1, X2, respectively. In each figure, the curves for different wavelengths are plotted with different colours and symbols. These three figures all demonstrate that, for different input wavelengths λ, the t_{op}/λ over L/λ curves align with each other very well except for the discrepancy near the first peak in Fig. 6(c). We attribute this to the dramatic intensity difference between the waveguide end facet and the X2 trapping point. These results clearly demonstrate the scaling effects of the optimal waveguide thickness and the gap distance over the optical wavelength. The scaling effect is intuitive because gap distance and waveguide thickness are both geometric parameters, so that we could shrink or enlarge the whole system for different wavelength to make the systems equivalent to each other.

Analogous to the findings in Section 4 for a wavelength of 1550nm, these curves also show that the normalised optimal waveguide thickness t_{op_nor} generally increases with the normalised gap distance L_{nor}, along with a periodic feature. The t_{op_nor} over L_{nor} curves reach their peaks when the normalised gap distance is $L_{nor} = L/\lambda$ =n+0.5, n=0,1,2…, which matches the standing wave condition of the dual-waveguide configuration. In comparison to the curves at the trapping point at the centre shown in Fig. 6(a), the curves in Fig. 6(b and c) start from $L_{nor} \approx 1.5$ and $L_{nor} \approx 2.5$, because the trapping points X1 and X2 only exist when the $L_{nor} \geq 1.5$ and $L_{nor} \geq 2.5$, respectively.

Fig. 6(d, e, and f) show the corresponding maximum field intensity as a function of the normalised gap distance $L_{nor} = L/\lambda$ at the trapping point at the centre, X1, X2, respectively. These curves also show clear periodic standing wave features which result from the interference effect. It is interesting to note that the larger optical wavelength leads to weaker trapping capability. This is obvious as larger optical wavelength λ means larger gap distance L in the case of the same normalized gap distance $L_{nor} = L/\lambda$, which gives rise to greater radiation loss within the gap. Therefore, shorter input wavelength is generally preferred when we want to introduce stronger trapping capability. Communication band 1550nm wavelength

laser is usually used in SOI waveguide platform owing to its easy accessibility and low waveguide propagation loss, while wavelength below 1200nm can not be used in SOI platform due to the high material absorption loss. Compared to the SOI platform, the previously used Si_3N_4 or Ta_2O_5 is transparent at visible wavelength 532nm, which can be used to enhance the trapping capability as has been analysed above. However, the fabrication complexity may hinder the use of them.

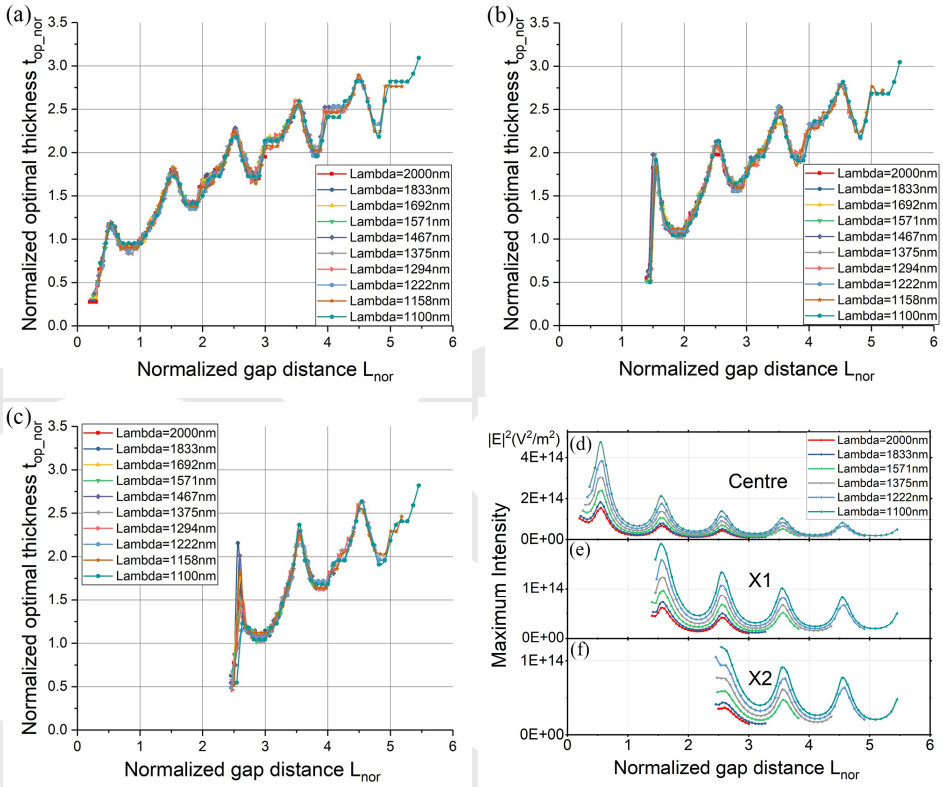

Fig. 6. (a, b and c) Normalised optimal waveguide thickness $t_{op\_nor} = t_{op}/\lambda$ as a function of the normalised gap distance $L_{nor} = L/\lambda$ at the trapping point at the centre, X1, X2, respectively. (d, e and f) Maximum intensity as a function of normalized gap distance L_nor=L/λ at the trapping point at the centre, X1, X2, respectively. In each figure, the curves for different wavelengths are plotted with different colours and symbols.

From the point of application, we always want to make the best of the input power and maximise the trapping capability within the gap. Further, we can adjust the gap distance or wavelength to meet the standing wave condition when the optical intensity reaches a local maximum. Thus, we here roughly summarise the value of normalised waveguide thickness t_{op_nor} for trapping points at the centre, X1, X2, when the standing wave condition is matched, namely the normalised gap distance $L_{nor} = L/\lambda$ =n+0.5, n=0,1,2…. We can only get a rough value of t_{op_nor} because they are not always precisely located in the standing wave points due to the discrete and limited number of positions in the simulations. The results are shown below in Table 1. We can see from Table 1 that when the gap distance matches the standing wave condition, the t_{op} is generally consistent with each other for the trapping points at Center, X1, and X2. There is a subtle difference among them, showing that the t_{op_nor} is slightly smaller when we want to trap a particle at the side rather than that at the centre. Furthermore, it is evident that a larger waveguide thickness is desired with larger gap distance, providing that the standing wave condition is fulfilled.

Table 1. The value of normalised optimal waveguide thickness t_{op_nor} when the Normalised gap distance match the standing wave condition, for trapping point at Center, X1 and X2

	normalised optimal waveguide thickness t_{op_nor}		
Normalised gap distance	Center	X1	X2
L_{nor}=0.5	1.2	--	--
L_{nor}=1.5	1.8	1.8	--
L_{nor}=2.5	2.25	2.2	2.1
L_{nor}=3.5	2.6	2.5	2.4
L_{nor}=4.5	2.9	2.8	2.6
….	…	…	…

6. Discussion and Conclusion

In summary, we present the design, optimisation and scaling effect of dual-waveguide optical traps on the SOI platform by comprehensive numerical simulations in Lumerical FDTD Solutions. In the simulations, two identical rib waveguides with two in-phase mode sources injected into opposite directions are designed to form a dual-waveguide optical trap. Within the gap, multiple interference maxima or hot spots can be formed, where the particles are trapped.

By studying the theoretical equations of optical force and trapping potential acting on a Rayleigh particle, we found that the trapping capability can be characterised by the optical intensity at the trapping location. The simulations demonstrate that the waveguide thickness is a crucial parameter in the design of dual-waveguide optical trap, and the optimal thickness depends on the gap distance between waveguides. The parametric sweep simulation found that the optimal waveguide thickness t_{op} increase with the gap distance L generally, and in the meantime is composited with periodic features whose period meets the resonance condition (standing wave in the gap). We also swept the wavelength from 1100nm to 2000nm and found that the optimal thickness shows a scaling effect over wavelength, meaning that the normalised optimal waveguide thickness t_{op_nor} shows the same features over normalised gap distance L_{nor}. The value of t_{op_nor} in various trapping points are summarised to provide explicit information on designing the optical trap.

This optimization result and the scaling effects show the fundamental relationship of waveguide thickness, gap distance, input wavelength when designing an on-chip dual-waveguide optical trap, and provide a comprehensive guidance to design such an optical trap. This will pave the way for further applications of dual-waveguide optical traps in biometric manipulation, Raman spectroscopy, on-chip levitated optomechanics, and integrated quantum photonics.

Funding

Engineering and Physical Sciences Research Council (EP/K000314/1); Royal Society (University Research Fellowship); Chinese Scholarship Council;

Acknowledgement

The authors would like to acknowledge Prof. Hendrik Ulbricht from the Department of Physics and Astronomy, University of Southampton for constructive discussions. The authors also acknowledge Prof. Goran Z. Mashnovich for useful feedbacks for this manuscript.

Disclosures

The authors declare no conflicts of interest.

References

1. A. Ashkin, "Acceleration and Trapping of Particles by Radiation Pressure," Physical Review Letters **24**, 156–159 (1970).
2. A. Ashkin, J. M. Dziedzic, J. E. Bjorkholm, and S. Chu, "Observation of a single-beam gradient force optical trap for dielectric particles," Optics Letters **11**, 288–290 (1986).
3. A. Ashkin, "History of optical trapping and manipulation of small-neutral particle, atoms, and molecules," IEEE Journal of Selected Topics in Quantum Electronics **6**, 841–856 (2000).
4. M. Bhattacharya, A. N. Vamivakas, and P. Barker, "Levitated optomechanics: introduction," Journal of the Optical Society of America B **34**, LO1–LO2 (2017).
5. J. Millen, T. S. Monteiro, R. Pettit, and A. N. Vamivakas, "Optomechanics with levitated particles," Reports on Progress in Physics 83, 026401 (2020).
6. D. Hempston, J. Vovrosh, M. Toroš, G. Winstone, M. Rashid, and H. Ulbricht, "Force sensing with an optically levitated charged nanoparticle," Applied Physics Letters **111**, 133111 (2017).
7. F. Monteiro, S. Ghosh, A. G. Fine, and D. C. Moore, "Optical levitation of 10 nanogram spheres with nano-g acceleration sensitivity," Physical Review A 96, 063841 (2017).
8. L.-M. Zhou, K.-W. Xiao, Z.-Q. Yin, J. Chen, and N. Zhao, "Sensitivity of displacement detection for a particle levitated in the doughnut beam," Optics Letters **43**, 4582–4585 (2018).
9. U. Delić, M. Reisenbauer, K. Dare, D. Grass, V. Vuletić, N. Kiesel, and M. Aspelmeyer, "Cooling of a levitated nanoparticle to the motional quantum ground state," Science 367, 892–895 (2020).
10. V. Jain, J. Gieseler, C. Moritz, C. Dellago, R. Quidant, and L. Novotny, "Direct Measurement of Photon Recoil from a Levitated Nanoparticle," Phys Rev Lett **116**, 243601 (2016).
11. A. Constable, J. Kim, J. Mervis, F. Zarinetchi, and M. Prentiss, "Demonstration of a fiber-optical light-force trap," Optics Letters **18**, 1867–1869 (1993).
12. P. R. T Jess, V. Garcés-Chávez, D. Smith, M. Mazilu, L. Paterson, A. Riches, C. S. Herrington, W. Sibbett, K. Dholakia, A. Ashkin, J. M. Dziedzic, J. E. Bjorkholm, and S. Chu, "Dual beam fibre trap for Raman micro-spectroscopy of single cells," Optics Express **14**, 5779–5791 (2006).
13. S. Kühn, E. J. Lunt, B. S. Phillips, A. R. Hawkins, and H. Schmidt, "Optofluidic particle concentration by a long-range dual-beam trap," Optics Letters **34**, 2306–2308 (2009).
14. B. S. Ahluwalia, A. Z. Subramanian, O. G. Hellsø, N. M. B. Perney, N. P. Sessions, and J. S. Wilkinson, "Fabrication of submicrometer high refractive index tantalum pentoxide waveguides for optical propulsion of microparticles," IEEE Photonics Technology Letters **21**, 1408–1410 (2009).
15. B. S. Ahluwalia, P. McCourt, T. Huser, and O. G. Hellesø, "Optical trapping and propulsion of red blood cells on waveguide surfaces," Optics Express **18**, 21053–21061 (2010).
16. S. Kawata and T. Sugiura, "Movement of micrometer-sized particles in the evanescent field of a laser beam," Optics Letters **17**, 772–774 (1992).
17. M. M. van Leest, F. Bernal Arango, and J. Caro, "Optical forces and trapping potentials of a dual-waveguide trap based on multimode solid-core waveguides," Journal of the European Optical Society **6**, 11022 (2011).
18. M. Boerkamp, T. van Leest, J. Heldens, A. Leinse, M. Hoekman, R. Heideman, and J. Caro, "On-chip optical trapping and Raman spectroscopy using a TripleX dual-waveguide trap," Optics Express **22**, 30528–30537 (2014).
19. G. B. Loozen and J. Caro, "On-chip optical trapping of extracellular vesicles using box-shaped composite SiO 2 -Si 3 N 4 waveguides," Optics Express **26**, 26985–27000 (2018).
20. A. Leinse, R. G. Heideman, E. J. Klein, R. Dekker, C. G. H. Roeloffzen, and D. A. I. Marpaung, "TriPleX^{TM} platform technology for photonic integration: Applications from UV through NIR to IR," 2011 ICO International Conference on Information Photonics, IP 2011 **4**, 1–2 (2011).
21. G. B. Loozen, A. Karuna, M. M. R. Fanood, E. Schreuder, and J. Caro, "Integrated photonics multi-waveguide devices for optical trapping and Raman spectroscopy: design, fabrication and performance demonstration," Beilstein J. Nanotechnol. **11**, 829–842 (2020).
22. O. G. Helleso, P. Lovhaugen, A. Z. Subramanian, J. S. Wilkinson, and B. S. Ahluwalia, "Surface transport and stable trapping of particles and cells by an optical waveguide loop," Lab on a Chip **12**, 3436–3440 (2012).
23. B. S. Ahluwalia and O. G. Hellesø, "Optical waveguide loop for planar trapping of blood cells and microspheres," Proc. of SPIE **8810**, 88100T (2013).
24. P. Løvhaugen, B. S. Ahluwalia, T. R. Huser, and O. Gaute Hellesø, "Serial Raman spectroscopy of particles trapped on a waveguide," Optics Express **21**, 2964–2970 (2013).
25. Ø. I. Helle, B. S. Ahluwalia, and O. G. Hellesø, "Optical transport, lifting and trapping of micro-particles by planar waveguides," Optics Express **23**, 6601–6612 (2015).
26. B. S. Ahluwalia, Ø. I. Helle, and O. G. Hellesø, "Rib waveguides for trapping and transport of particles," Optics Express **24**, 4477–4487 (2016).
27. "Nanophotonic FDTD Simulation Software - Lumerical FDTD," https://www.lumerical.com/products/fdtd/.
28. G. Reed and A. Knights, *Silicon Photonics: An Introduction* (2004).
29. H. A. Haus, Waves and Fields in Optoelectronics (Prentice-Hall, 1984).
30. "Optical force on a particle – Lumerical," https://support.lumerical.com/hc/en-us/articles/360042214494-Optical-force-on-a-particle-2D-.

31. Y. Harada and T. Asakura, "Radiation forces on a dielectric sphere in the Rayleigh scattering regime," Optics Communications **124**, 529–541 (1996).